NASA
Technical
Paper
2162

May 1983

Experimental Verification of the Multistage Depressed Collector Design Procedure for a High-Perveance, Helix-Type, Traveling-Wave Tube

James A. Dayton, Jr.,
Henry G. Kosmahl,
and Peter Ramins

NASA

25th Anniversary
1958-1983

NASA
Technical
Paper
2162

1983

Experimental Verification of the Multistage Depressed Collector Design Procedure for a High-Perveance, Helix-Type, Traveling-Wave Tube

James A. Dayton, Jr.,
Henry G. Kosmahl,
and Peter Ramins
Lewis Research Center
Cleveland, Ohio

NASA
National Aeronautics
and Space Administration
**Scientific and Technical
Information Branch**

Summary

The validity of a computational procedure for the design of multistage depressed collectors (MDC's) is demonstrated for a traveling wave tube (TWT) with a perveance of 1.23×10^{-6}. The MDC is used with spent-beam refocusing to improve substantially the efficiency of the TWT. Previous reports on this subject have verified, under a variety of operating conditions, the MDC design procedure for TWT's with lower perveance.

The design procedure is based on two computer programs that create a mathematical model of the electric and magnetic fields of the TWT-refocuser-MDC system and its electron beam. The two principal outputs of the analysis are a description of the radiofrequency (rf) performance of the TWT and the trajectories of representative groups of charges from the input of the TWT to their points of interception on the MDC electrodes. The trajectories provide the information from which the collector efficiency can be calculated.

The analytical predictions were compared in considerable detail with measured results. Very good agreement was obtained between the analytical and experimental values of collector efficiency. Several design iterations are described. The highest experimentally optimized MDC efficiencies achieved were 79 percent for a five-stage collector and 78 percent for a four-stage collector. The collecting surfaces of the MDC were contained within a cylindrical volume approximately 2.4 centimeters in diameter and 3.0 centimeters long.

Introduction

This paper presents the latest experimental and analytical results from a joint USAF-NASA program that has been conducted at the Lewis Research Center since 1974. The program's goal is to apply to electronic countermeasure systems the multistage depressed collector (MDC)(refs. 1 and 2) and spent-beam-refocusing techniques (refs. 3 and 4) developed by NASA for the improvement of the efficiency of traveling wave tubes (TWT's) in communications satellites. The results reported here for Varian Associates TWT No. 6336 extend to 1.23×10^{-6} the range of perveance over which the analytical and experimental methods for the study of the MDC and spent-beam refocuser have been found to be in substantial agreement. Previous results, obtained for perveances of 0.5×10^{-6} and lower, have demonstrated excellent agreement between measured performance and analytical prediction of the MDC efficiency for single- and dual-mode, octave-bandwidth TWT's (refs. 5 to 8) over a range of output powers from saturation to several decibels below (refs. 7 and 8).

The analytical portion of this work has been described in detail in previous publications (refs. 5 and 6). One computer program is used to analyze the flow of electrons through the slow wave circuit of the TWT, providing a large signal analysis of the TWT performance and an analysis of the distribution of the vector velocity and position of electrons in the spent beam. The second program, due to Herrmannsfeldt (ref. 9), is used to analyze the motion of the electron beam in the refocuser and MDC. The validity of this design procedure having been established, the use of these two computer programs can reduce considerably the number of experimental iterations needed to achieve a new design.

The experimental phase of the program has also been described in detail previously (ref. 10). Detailed measurements are made of the current flow and power flow within the TWT and MDC being tested. The data are recorded and analyzed by computer in real time, and the system response to various parameters can be determined promptly and in detail.

Described in this report are six design iterations and the rationale on which they were based. Not all of these iterations were strictly necessary to achieve the final result but were undertaken in part because of the availability of collector electrodes and testing facilities. However, the specialist in this field may find the information obtained to be of interest.

Analytical Program

Overall System

Flow diagrams illustrating the distributions of power and electron current are shown in figure 1 for the TWT-refocuser-MDC system. The definitions of collector efficiency and of the various components of power are also presented in this figure. For the purpose of analysis, the system was divided into four parts: (1) the TWT between the rf input and output; (2) a drift region past the rf output in a continuation of the focusing magnetic field; (3) the refocusing region; and (4) the MDC.

The first two parts of the calculation were performed using the Lewis Research Center's large-signal, multidimensional, helical TWT program. In this program the electron beam is divided into 32 disks of charge per rf cycle, and the trajectories of the disks are tracked through the tube. In parts (3) and (4) of the calculation, the trajectories of the 32 representative charges were computed using the Herrmannsfeldt program.

Traveling Wave Tube

In the TWT, disk trajectories in the presence of rf circuit forces, space charge forces, and magnetic focusing

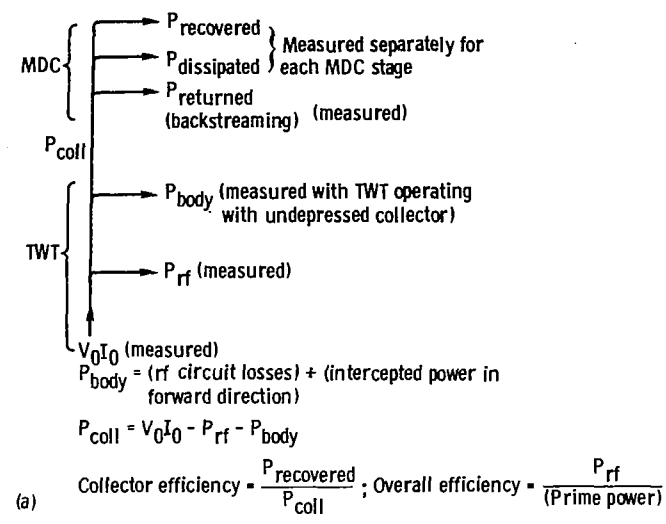

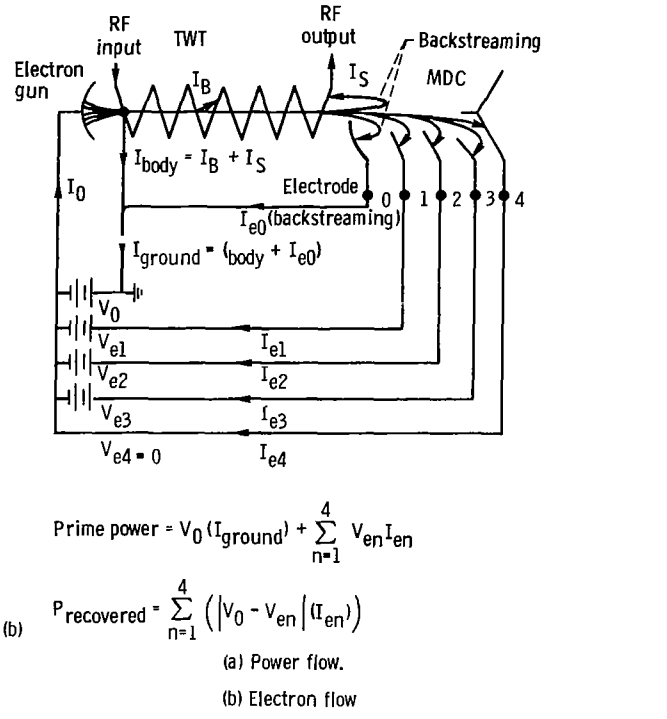

(a) Power flow.

(b) Electron flow

Figure 1. - Flow diagrams for TWT with four-stage depressed collector.

fields are computed from the rf input of the TWT to the rf output.

At the rf output the computer program lists the following:

(1) rf output power
(2) rf circuit losses
(3) Sever and attenuator losses
(4) Intercepted current and power
(5) Radial coordinates of the disk edges
(6) Three components of velocity ($\dot{r}$, $\dot{\varphi}$, $\dot{z}$) of each disk
(7) Relative phase of each disk.

The trajectory program does not include effects of thermal velocities on the radial and azimuthal motion. According to Herrmann's optical theory of thermal electrons, these effects should be negligible for a tube such as this with a perveance of 1.23×10^{-6}.

At the rf output the electron beam is tightly bunched, causing strong space charge forces to exist between disks. If the beam is permitted to drift beyond the rf output while remaining under the control of the focusing magnetic fields, these space charge forces will cause the beam to debunch, with the result that the distribution of velocities will be more narrow and the current density as a function of time, more uniform.

Refocusing System

The description of the spent beam at the end of the drift region provides the input data for the refocusing system calculations. The computation of the trajectories in the refocuser and in the MDC treats the 32 disks as continuous rays of current, that is to say, complete debunching is assumed. Each current ray is located at the centroid of charge of its corresponding disk and has the vector velocity of the disk centroid. Current ray trajectories in the presence of the magnetic refocusing fields and space charge are computed throughout the refocuser. The beam characteristics (current ray position coordinates and vector velocities) at the end of the refocusing define the input conditions to the MDC.

Multistage Depressed Collector

In the MDC analysis the trajectory calculation is continued until the current rays impact the MDC electrodes. The effects of secondary electron emission can only be estimated. It is assumed that all charge impacts on the MDC electrodes generate only low-energy secondaries, with the local electric field determining whether they are suppressed or accelerated to less depressed electrodes. In these calculations a yield of 0.4 secondary electrons per primary electron was used since a coating of carbon black (soot) was used on the experimental collector electrodes. Based on the entrance conditions and the point of collection of each ray, a calculation is made of the collected current, recovered power, and dissipated power at each of the collector electrodes and, if backstreaming occurs, at the TWT itself. These results, when coupled with the outputs of the TWT computer program, provide a detailed picture of the current and power flow within the TWT-MDC system.

Because of the close proximity of the first depressed stage to the end of the refocusing tunnel, the MDC analysis was begun inside the tunnel so that the potential depression within the tunnel due to the first stage could be accounted for more accurately.

Experimental Program

The experimental program was designed to measure the various powers, currents, and voltages shown in the power flow and electron flow diagrams (fig. 1), permitting a detailed comparison with the analytical results. The experimental techniques are described in detail in reference 10.

General Characteristics

Frequency, GHz	2.5 to 5.5
Beam voltage, kV	6.2
Beam current, A	0.600
Perveance, $A/V^{3/2}$	1.23×10^{-6}
Electronic efficiency, percent of maximum (4.75 GHz)	26
Duty cycle	rated CW[a]
Focusing	ppm

[a]limited to 25 to 50 percent during these tests

As implied by the table above, all measurements reported here were obtained by pulsed operation of the TWT. Because of the large intercepted beam current, CW operation was not attempted. As in previous tests, a valve was used to keep the TWT under hard vacuum while the MDC was being modified; nonetheless, some differences in tube performance were observed from test to test. Soot was used on all MDC electrode surfaces to suppress secondary electron emission.

Measurements of the dissipated power in each stage of the MDC apparently were complicated by radiative heat transfer between electrodes. Some soot-coated electrode surfaces were observed to glow when bombarded by the electron beam. In particular, the most depressed stage seems to dissipate more power than would be expected from the very small measured current to this electrode. Even when a direct-current electron beam is injected into the collector and virtually no current is being collected on the most depressed stage, there is significant measured dissipation there.

Results for the Helical TWT Program

Slow Wave Circuit

The large-signal computer program has been found consistently to produce accurate numerical simulations of a general tube type; however, any particular tube of the type may have operating characteristics that differ from the general type. In the case of the VA6336, the preliminary data, on which the large signal TWT analysis and the first refocuser and MDC designs were based, indicated an operating voltage of 5.8 kilovolts and a current of 550 milliamperes, while the actual tube, delivered some time later, operated at 6.2 kilovolts and 600 milliamperes.

This discrepancy in current was magnified by one of the characteristics of the VA6336 that could not be modeled by the computer program, the modulating grid in the tube's electron gun. An initial condition for the electron beam in the large-signal helical TWT program is that the electron beam be of uniform current density and zero injection angle, an idealization that is a good engineering approximation to the real beam for many applications. However, the grid of the VA6336 interferes with the formation of a uniform beam, an effect that manifests itself in a larger body current and in a lower electronic efficiency than predicted by the computer. This indicated that the beam perturbation due to the grid was resulting in substantial beam interception well before the output, that is, before appreciable rf interaction had taken place. In an attempt to simulate this beam interception, the computation was redone with a beam current of only 510 milliamperes at 5.8 kilovolts, with the result that reasonable agreement with experiment was obtained for rf output power, gain, and electronic efficiency. In the analysis of the MDC discussed later in this report, the discrepancy between the beam current in the actual tube and the mathematical model of the tube was treated by presenting the various voltages, currents, and powers as percentages of the respective beam voltage, current, and power.

Sometime after the computer analysis of the VA6336 with refocuser and MDC had been completed, experimental data were obtained that indicated that the circuit efficiency in the actual tube was approximately 87.3 percent. Since the circuit efficiency used in the computation was 93.3 percent, the actual circuit losses appear to be approximately twice as great as those used in the computation. If the computation were to be redone with the lower circuit efficiency, it might be expected to result in a lower rf output power and electronic efficiency for the same beam current, possibly bringing the calculated results into better agreement with the experimental measurements. However, this approach was not pursued because the experimental and analytical work on this tube had been nearly completed.

The large-signal computer analysis was done at the midband frequency of 4.0 gigahertz, where the greatest electronic efficiency was expected to occur. Multistage depressed collector designs are typically optimized for the frequency of greatest electronic efficiency because it is there that the greatest disorder is found in the spent electron beam and the greatest direct current input power is drawn. Subsequently, it was discovered that the maximum electronic efficiency actually occurred at 4.75 gigahertz. Although the analysis was not repeated, each collector design was experimentally optimized at this frequency by adjusting the collector voltages, spike length, and magnetic refocusing.

The spent-beam kinetic energy distribution at the rf output is shown in figure 2. The energy distribution at the input to the refocuser after the beam has drifted through 1¼ magnetic periods beyond the rf output is presented both as the kinetic energy only and as the sum of the kinetic and potential energy. It can be seen that the debunching that occurs in the drift in the absence of the rf fields tends to slow down the most energetic electrons and to speed up the slowest, enhancing the effectiveness of the MDC. The total energy distribution represents the entire energy content of the spent beam as it enters the refocuser-MDC system.

Refocusing Analysis Results

By permitting the slow expansion of the beam, the refocusing system converts to kinetic energy some of the potential energy contained in the beam space charge and reduces the magnitudes of the angles the current rays make with the tube axis. In this study an attempt was made to design a refocusing system analytically rather than empirically. The result of this exercise can be seen in figure 3 and table I(a). The beam was allowed to approximately double in diameter and the large positive angles present at the input of the refocuser were substantially reduced or made negative. There are a number of large negative angles in the beam at the output of the refocuser, but these were thought to be beneficial to the operation of an MDC of this small size and aspect ratio. However, the refocusing design was completed long before all of the pole piece dimensions were finalized, and the magnetic profile required to achieve this design was not physically realizable. An MDC was

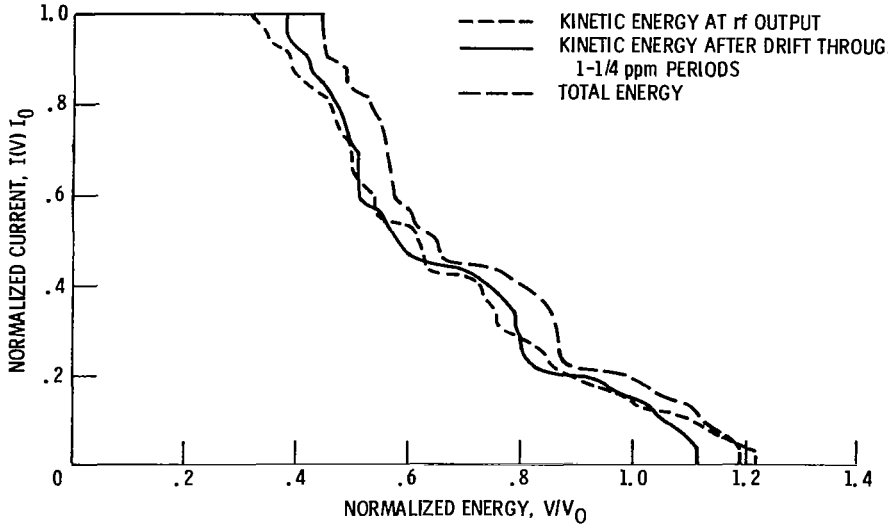

Figure 2. - Computed spent-beam energy distributions at saturation. Electronic efficiency, η_e, 0.273; perveance, 1.15×10^{-6} $A/V^{3/2}$.

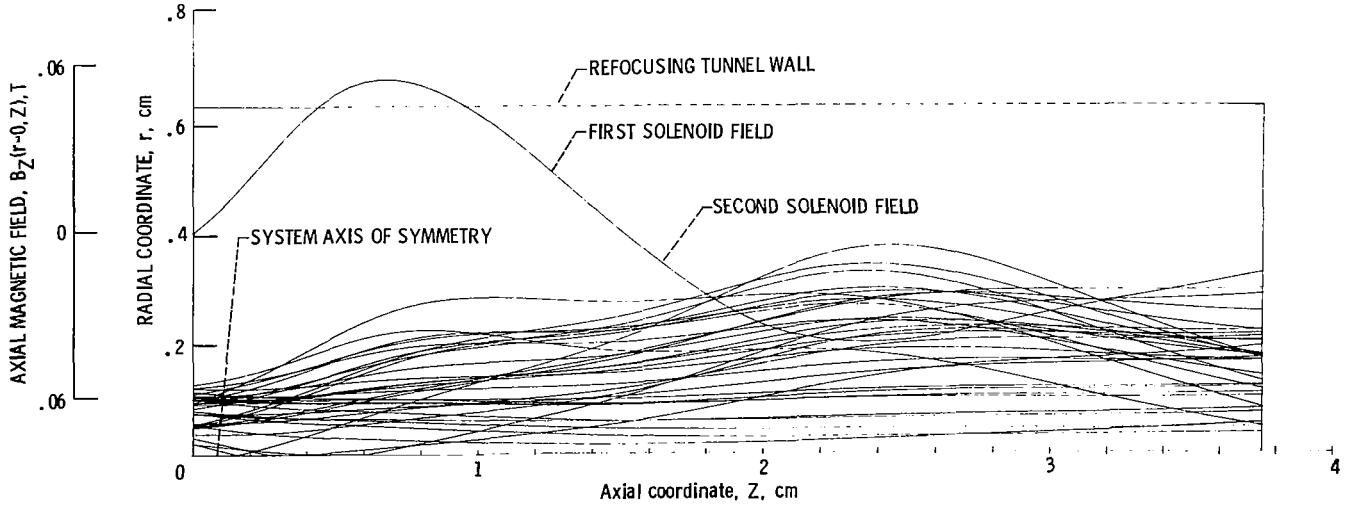

Figure 3. - Charge trajectories and refocusing field profile (analytical design case) in refocusing section for TWT operation at saturation.

designed based on this refocuser and will be presented in the next section of this report. This analytical refocuser and MDC design is included in this report because the MDC was built, tested, and modified during the course of the program.

An analysis of the actual refocusing profile used is presented in figure 4 and table I(b.) The magnetic profile was optimized empirically for the first case tested and analyzed using the method described by Stankiewicz (ref. 11). This refocusing magnetic profile was used for all comparisons of analytical and experimental performance, although it was optimum for only the first. However, the optimized profiles for the other cases (experimental optimizations at 4.75 GHz) appeared to deviate from this by only a few percent. The beam diameter was permitted to triple in this refocuser, and there are fewer very large or very small angles present than for the analytical refocuser.

The spent-beam energy distribution at the input to the MDC, computed using the empirical refocusing profile, is shown in figure 5 compared with the distribution at the rf output. The effect of the refocuser has been to bring the energy distribution entering the MDC closer to the total energy distribution shown in figure 2.

MDC Analysis Results and Comparison with Experimental Measurements

Analytical Design

The first MDC design was based on the refocusing system (fig. 3) that was subsequently found to be physically unrealizable. The trajectories of the 32 current rays and the equipotential lines are shown on a drawing of the cross section of this MDC in figure 6. The electrode surface cross sections have been shaded and marked with their potential in volts with respect to ground. The equipotential lines are labeled in fractions of the cathode potential. The analysis of the TWT and this MDC, predicting a collector efficiency of 74.8 percent and an overall efficiency of 54.5 percent, is presented in

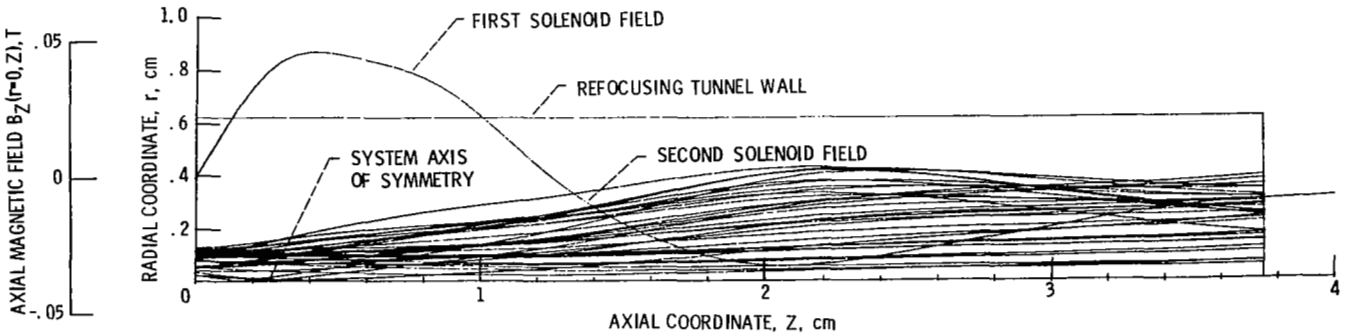

Figure 4. - Charge trajectories and refocusing field profile (experimentally optimized) in refocusing section for TWT operation at saturation.

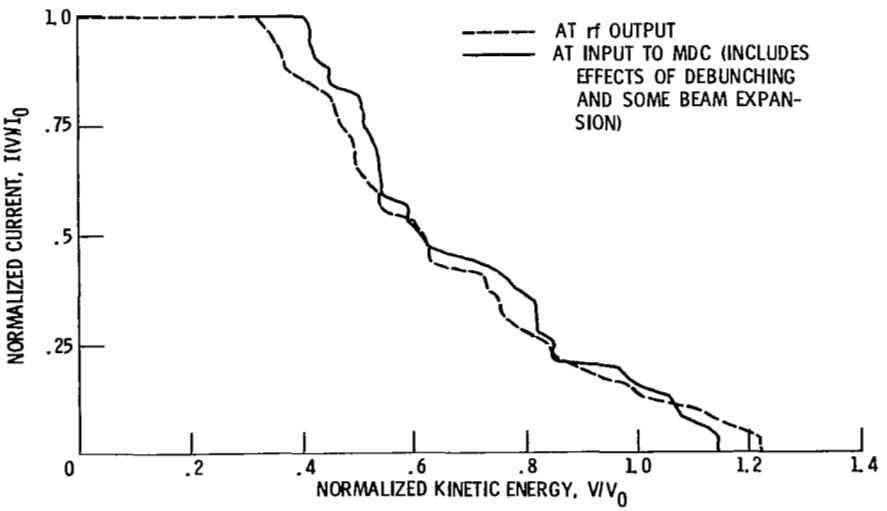

Figure 5. - Computed spent-beam energy distributions at saturation, showing the effects of beam refocusing. Electronic efficiency, η_e, 0.273, perveance, 1.15×10^{-6} $A/V^{3/2}$

table II. There is, of course, no experimental comparison available. In this and all analyses presented in this report, the secondary yield for the soot-covered electrode surfaces was 0.4, and the distribution of secondary electrons was determined from the electrode geometry and the electric fields in the vicinity of the impact.

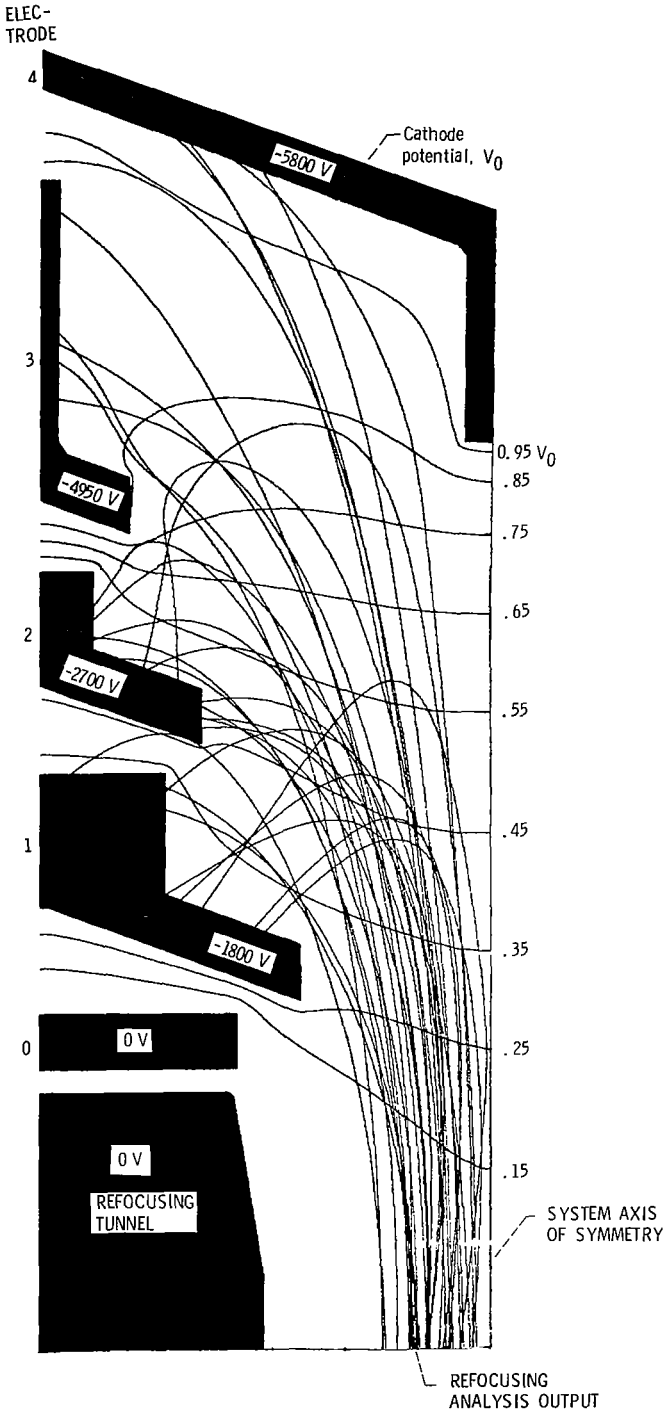

Figure 6. - Charge trajectories in four-stage, 2.4-centimeter-diameter, depressed collector (first design). Design case with projected (but not realizeable) refocusing field profile; TWT operating at saturation.

When this collector was used with the experimentally optimized refocusing system (fig. 4), the result was a substantially lower collector efficiency. The experimentally optimized refocusing system was subsequently programmed, and the collector performance recomputed. The analysis indicated that the experimentally optimized refocuser produced a larger diameter electron beam, which resulted in considerable interception at the aperture of the first stage, causing the reduced collector efficiency. The trajectories obtained for the first design using the experimentally optimized refocusing system are shown in figure 7. The analysis of this computation and a comparison with the measured results are presented in table III. Both the current distribution and the collector

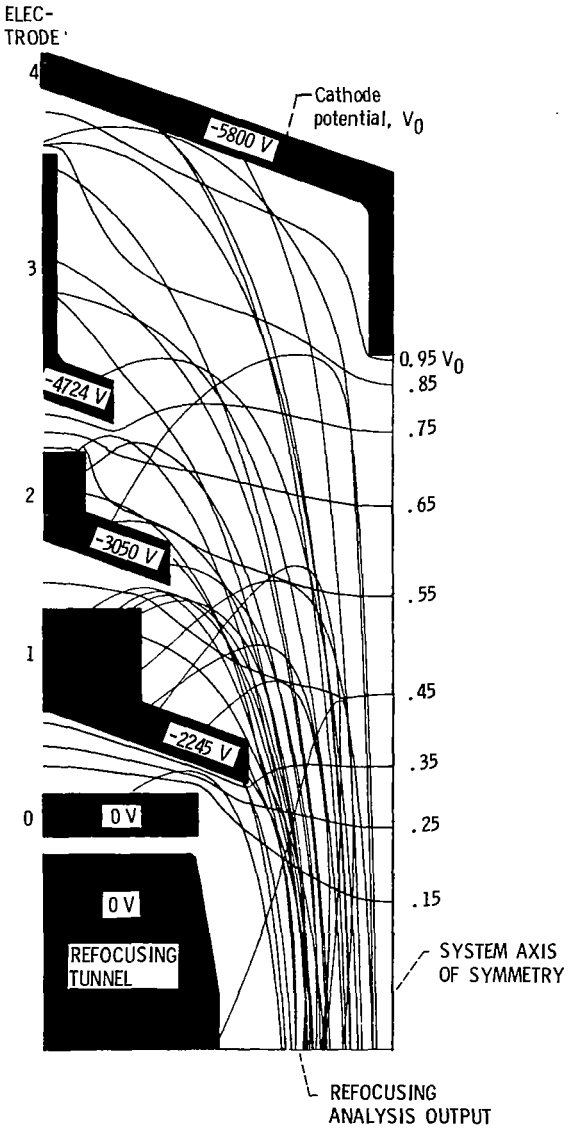

Figure 7. - Charge trajectories in four-stage, 2.4-centimeter-diameter, depressed collector (first design). TWT operating at saturation.

efficiency are in good agreement. As discussed previously, the currents, voltages, and powers are all presented as percentages of the respective cathode current, cathode voltage, and beam power. When fully optimized, a collector efficiency of 71.6 percent was obtained.

Second Design

By enlarging the apertures of the first two depressed stages, the computer analysis predicted that the collector efficiency would improve to 73.5 percent. The trajectories for this second design are shown in figure 8, and the experimental and analytical results are shown in table IV. The measured collector efficiency did improve but only to 71.3 percent. Also, the agreement between measured and analytical collector currents is not as good as for the first design. The optimum experimental efficiency for this configuration, obtained as described in a previous section, was 73.4 percent.

Third Design

The third collector design used in this study was based on existing parts of one that had been a previous design for a dual mode TWT (refs. 7 and 8). Modifications were made to the collector to accommodate the more dispersive spent beam encountered on this tube. The second- and third-stage electrode apertures were enlarged, and the ground potential electrode separating the first depressed electrode and the tube body was eliminated. The computed trajectories for this case are shown in figure 9, and the experimental and computed results are presented in table V.

The computed results indicated that this MDC would be slightly less efficient than the second design, and indeed the measured collector efficiency was slightly

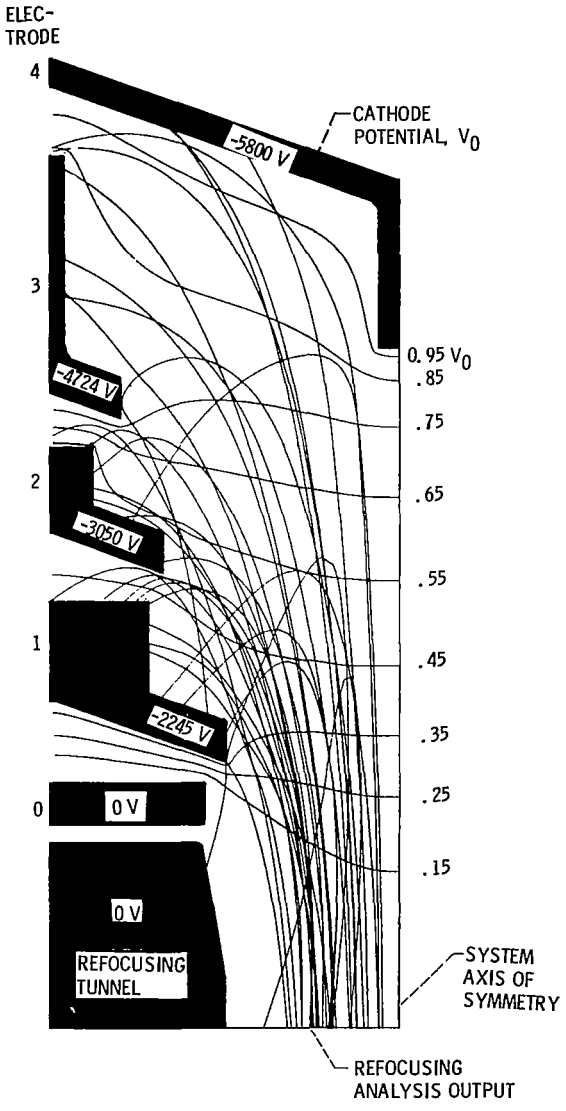

Figure 8. - Charge trajectories in four-stage, 2.4-centimeter-diameter, depressed collector (second design) TWT operating at saturation.

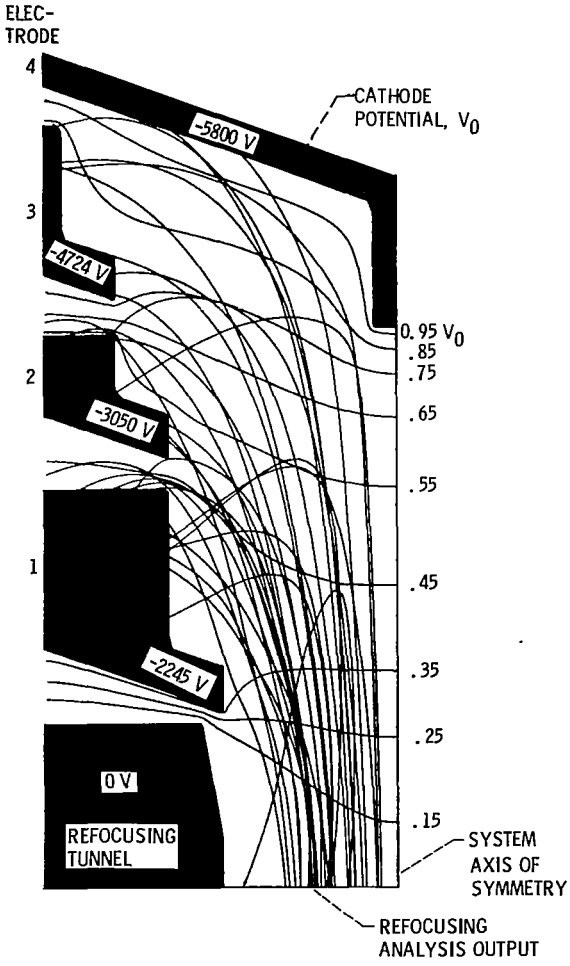

Figure 9. - Charge trajectories in four-stage, 2.4-centimeter-diameter, depressed collector (third design). TWT operating at saturation.

lower. The current distribution to the collector plates is in reasonable agreement, but the measured collector efficiency of 70.2 percent is 2.8 percentage points lower than the computed value. However, when experimentally optimized, this MDC had an efficiency of 74.2 percent.

Fourth Design

In the fourth design an attempt was made to improve the MDC efficiency by collecting at the second depressed stage the current that had been incident on the upper side of the first stage (figs. 8 and 9). These current rays had sufficient energy to reach the second stage but had been unable to do so because of excessive dispersion in the lower end of the MDC. Figure 10 shows how this was accomplished.

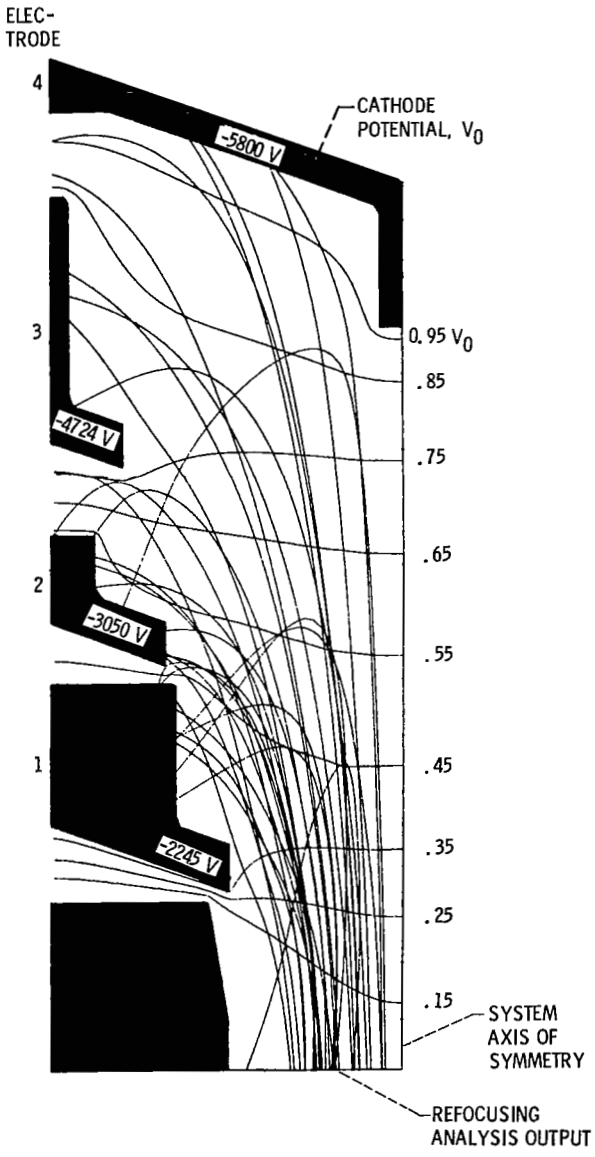

Figure 10. - Charge trajectories in four-stage, 2.4 centimeter-diameter, depressed collector (fourth design). TWT operating at saturation.

The ground potential buffer electrode was removed. This does not reduce the dispersion of the collector but does shorten the distance traveled to a depressed stage and, generally, the radial deflection also. The first depressed stage used in the third design (fig. 9) was shortened slightly, and the second and third stages were those used in design two (fig. 8). The second depressed stage, which had an entrance aperture larger than the trailing aperture of the first stage, was brought as close to the first stage as high voltage consideration would permit. With the second stage in this position, its dispersive effect was minimized, and the desired effect of shifting some of the current to stage 2 from stage 1 was achieved.

Reducing the dispersion at the lower end of the collector had the undesirable effect of providing inadequate dispersion to the high-energy rays impacting the fourth stage. This was countered by increased spacing between the upper stages, thereby increasing the axial travel of the electrons and causing them to impact further from the axis.

An analysis of this design is presented in table VI. Both the predicted and measured collector efficiencies were improved by this design and were in slightly better agreement. Also, both the experimental and measured results showed a decrease in the current to the first depressed stage and an increase at the second stage when compared with table IV. When experimentally optimized, this MDC had an efficiency of 76.3 percent.

Fifth Design

The fifth collector design was intended to reduce the losses due to the secondary emission from the second depressed stage aperture and the top plate. To accomplish this, the upper three stages were redesigned (fig. 11).

To insure that secondary emission from the top plate would be directed to the third depressed stage, the diameter of the third stage aperture was reduced and a conical section was added to the top plate surrounding the spike. The conical section had the effect of forcing electrons incident on the top plate to impact at larger radii, trapping the resulting secondaries above the smaller, third-stage aperture.

At the second depressed stage aperture, it was necessary to reduce the potential depression due to the third stage, an effect that would now be more pronounced because of the reduction in the third-stage aperture. This was accomplished by lengthening the second stage and reducing the diameter of the vertical section to the same diameter as the third-stage aperture.

The analysis predicted an MDC efficiency of 78.0 percent, an improvement of 1.2 percentage points over the fourth design. As can be seen from table VII, this was realized experimentally. When fully optimized, this collector had a measured efficiency of 77.4 percent.

Sixth Design

The current to the second depressed stage in the MDC designs described above appears to be separated into two distinct energy classes: one impacting the entrance aperture, and the other the upper region of the vertical section. This suggests that the efficiency of the MDC might be improved by the introduction of an additional depressed stage, effectively dividing the second stage in two.

This five-stage MDC was attempted as the sixth design; the result is shown in figure 12, and an analysis is presented in table VIII that predicts an MDC efficiency of 80.1 percent. An improvement over design 5 of 2.1 percentage points was predicted, but an improvement of only 0.8 percentage point was measured. However, when this design was optimized, the measured MDC efficiency was 79.0 percent, and the overall efficiency was 50 percent.

This same collector was operated as a four-stage MDC by electrically connecting the second and third stages. The analysis presented in figure 13 and table IX predicts a collector efficiency of 78.4 percent, worse than for the five-stage MDC, but slightly better than the four-stage MDC (shown in fig. 11 and table VII). The measured value of collector efficiency was 76.1 percent for the conditions of the analysis and 78.0 percent (49 percent overall) when experimentally optimized.

Experimental Optimization of Collector Efficiency

As described previously, the MDC efficiency was experimentally optimized at 4.75 gigahertz, the frequency

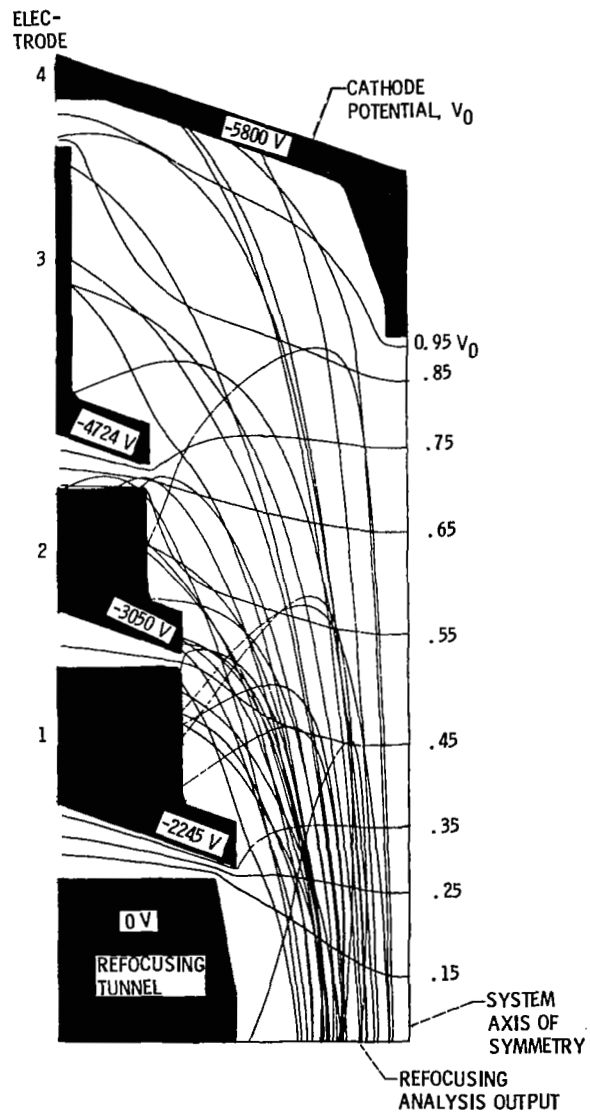

Figure 11. - Charge trajectories in four-stage, 2.4 centimeter-diameter, depressed collector (fifth design). TWT operating at saturation.

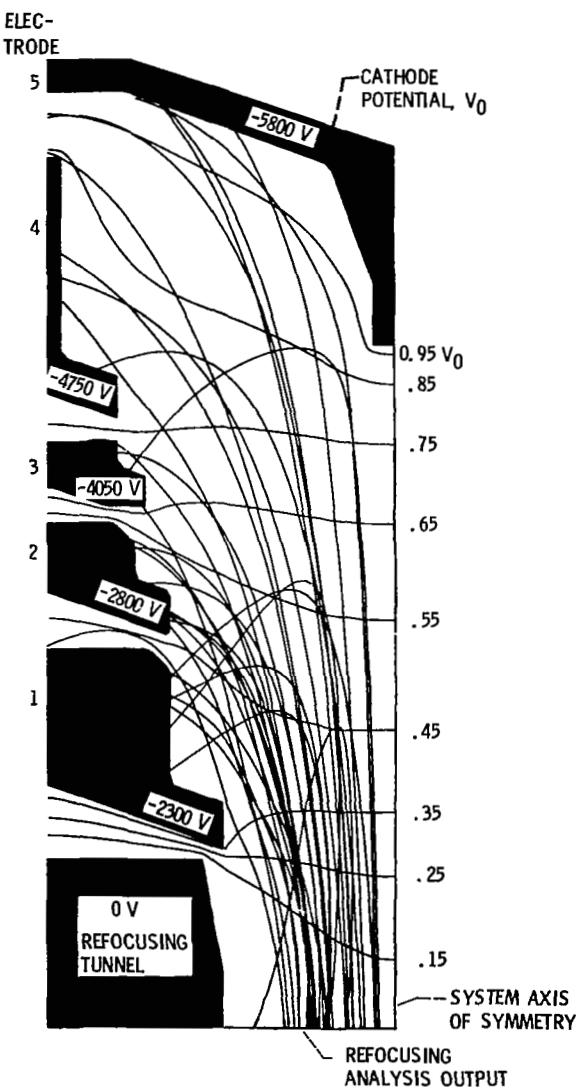

Figure 12. - Charge trajectories in five-stage, 2.4-centimeter-diameter, depressed collector (sixth design). TWT operating at saturation.

of maximum electronic efficiency and, therefore, usually maximum direct-current input power. This optimization is accomplished by manipulating the system parameters that are readily accessible, the collector voltages, spike length, and refocuser magnetic fields. The results of optimization are summarized in table X.

Although a refocuser optimization was obtained for each MDC design, it was felt that the analysis would have been unduly complicated by recomputing each analytical case with the empirically obtained optimum focusing field. Therefore, all analytical results were based on the optimum refocuser for the first design. This procedure was acceptable because it was observed experimentally that the refocuser optimizations after the first design were only slightly different from each other and produced only small improvements in MDC efficiency. Although this spent-beam reconditioner comprised electromagnetic coils, some degree of adjustment of the refocusing profile would be possible even for a system with permanent magnets.

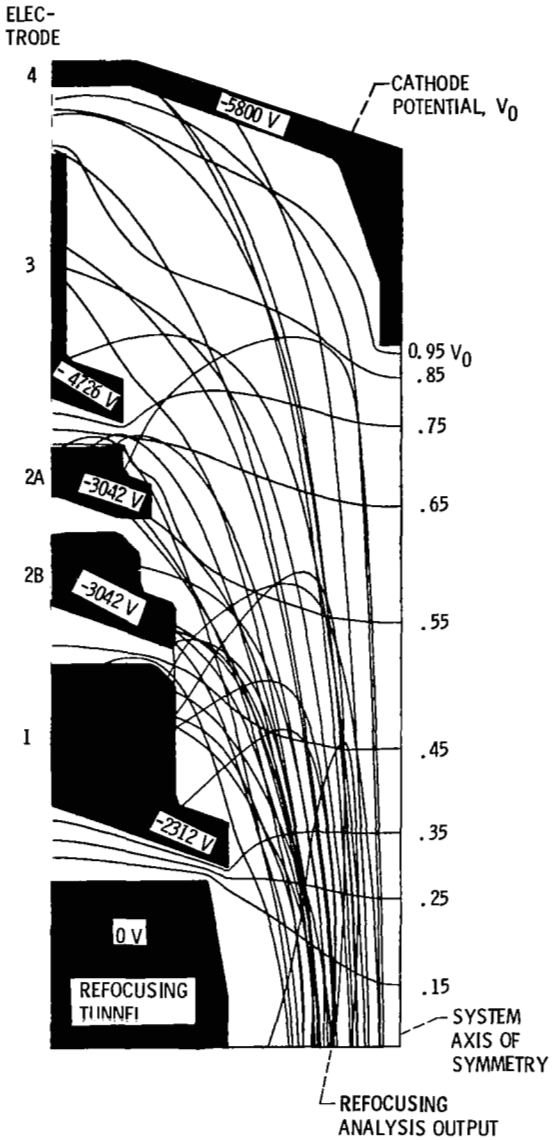

Figure 13. - Charge trajectories in four-stage, 2.4 centimeter-diameter, depressed collector (sixth design operated as a four-stage). TWT operating at saturation.

Concluding Remarks

The results presented here demonstrate a favorable comparison of the experimentally and analytically determined MDC efficiencies for a helical TWT operated at a microperveance of 1.23. This agreement is particularly good between the analytically predicted and experimentally optimized MDC efficiencies (table X). In work reported previously, similar agreement had been demonstrated for TWT's operated at lower perveances; the present results extend to the 1.23 microperveance regime, the range in which these analytical techniques can be confidently applied to MDC design.

The large number of designs undertaken in this study resulted more from the availability of compatible collector electrodes than from practical necessity. An adequate design ought to be achieved with fewer iterations with most of the optimization accomplished on the computer.

As in studies reported previously, the collector current distribution is in good agreement in only some cases. It needs to be remarked that the analytical current is divided into 32 rays of equal current, so that the resolution of the computed collector current distribution could be no better than 3.1 percent of the beam current. Further, an intercepted beam current of 6 percent was measured at rf saturation, while none was predicted analytically. This discrepancy in the intercepted beam current, which was discussed previously, had no effect on the comparison of collector efficiencies, but had a direct effect on the overall efficiency and made impossible an exact agreement of the measured and computed collector current distributions.

One third of the computed electrode currents agreed with measured values within one ray (3.1 percent of the beam current) and a second one-third are within two rays. Most of the larger discrepancies in electrode currents are due to relatively small discrepancies in the energy distribution in the spent beam. For example, in tables VI, VII, and IX the measured and computer currents to electrodes 2 and 3 disagree substantially, but the sums of the currents to electrodes 2 and 3 are in fair agreement. Similarly, the analysis consistently overestimates the current to the spike plate and underestimates the current to the next lower stage, while the sums of the two currents are in fair agreement. These discrepancies in current to adjacent electrodes introduce only minor errors in the computation of MDC efficiency.

At any rate, the primary concern in the design of an MDC is the collector efficiency, which is relatively insensitive to tube operating parameters, not the distribution of currents to the collector electrodes, which varies considerably with tube operating conditions. Regardless of the computer current distribution at one particular operating point, it would be necessary to design the collector to tolerate a wide range of current distributions to allow for operation under other conditions.

The overall efficiency for the fully optimized tube-refocuser-MDC system was 50 percent for the five-stage MDC and 49 percent for the four-stage UDC. With the beam transmission losses eliminated, the TWT overall efficiency could be approximately 60 percent.

Lewis Research Center,
National Aeronautics and Space Administration,
Cleveland, Ohio, December 6, 1982

References

1. Kosmahl, H. G.: A Novel, Axisymmetric, Electrostatic Collector for Linear Beam Microwave Tubes. NASA TN D-6093, Feb. 1971.
2. Kosmahl, H. G.; and Ramins, P.: Small-Size 81- to 83.5-Percent Efficient 2- and 4-Stage Depressed Collectors for Octave-Bandwidth High-Performance TWT's. IEEE Trans. Electron Devices, vol. ED-24, no. 1, Jan. 1977, pp. 36–44.
3. Kosmahl, H. G.: An Electron Beam Collector. U.S. Patent No. 3,764,850, Oct. 1973.
4. Stankiewicz, N.: Analysis of Spent Beam Refocusing to Achieve Optimum Collector Efficiency. IEEE Trans. Electron Devices, vol. ED-24, no. 1, Jan. 1977, pp. 32–36.
5. Dayton, J. A., Jr.; et al.: Analytical Prediction with Multidimensional Computer Programs and Experimental Verification of the Performance, at a Variety of Operating Conditions, of Two Traveling Wave Tubes with Depressed Collectors. NASA TP-1449, May 1979.
6. Dayton, J. A., Jr.; et al.: Analytical Prediction and Experimental Verification of TWT and Depressed Collector Performance Using Multidimensional Computer Programs. IEEE Trans. Electron Devices, vol. ED-26, no. 10, Oct. 1979, pp. 1589–1598.
7. Dayton, J. A., Jr.; et al.: Analytical Prediction and Experimental Verification of Performance at Various Operating Conditions, of a Dual-Mode Traveling Wave Tube with Multistage Depressed Collectors. NASA TP-1831, July 1981.
8. Dayton, J. A., Jr.; et al.: Experimental Verification of a Computational Procedure for the Design of TWT-Refocuser-MDC Systems. IEEE Trans. Electron Devices, vol. ED-28, no. 12, Dec. 1981, pp. 1480–1489.
9. Herrmannsfeldt, W. B.: Electron Trajectory Program. SLAC-166, Stanford Linear Accelerator Center, 1973.
10. Ramins, P.; and Fox, T.A.: Multistage Depressed Collector with Efficiency of 90 to 94 Percent for Operation of a Dual-Mode Traveling Wave Tube in the Linear Region. NASA TP-1670, Apr. 1980.
11. Stankiewicz, N.: A Matrix Solution for the Simulation of Magnetic Fields with Ideal Current Loops. IEEE Trans. Electron Devices, vol. ED-26, no. 10, Oct. 1979, pp. 1598–1601.

TABLE I. - INPUT AND OUTPUT ANGLES OF REFOCUSING SYSTEM FOR SATURATED OPERATION

(a) With analytical design profile

Trajectory[a]	Input angle,[b] deg	Output angle,[c] deg
1	3.8	-4.4
2	0	1.1
3	6.4	-7.6
4	-7.0	-8.0
5	4.8	-5.7
6	-2.7	3.6
7	7.2	-6.3
8	4.4	-4.1
9	-4.0	1.9
10	.5	1.8
11	2.3	3.4
12	10.7	-7.7
13	-.1	-.3
14	-6.1	2.3
15	3.0	-.5
16	4.4	-3.5
17	.2	1.8
18	3.7	2.1
19	-1.4	.2
20	.6	.9
21	-4.0	1.2
22	-3.6	.5
23	.3	1.1
24	-2.8	1.2
25	3.8	.7
26	-1.3	.7
27	-.4	1.6
28	-2.8	.7
29	-2.8	.4
30	-2.1	.9
31	-1.8	.8
32	-1.9	1.1

(b) With experimentally optimized profile

Trajectory[a]	Input angle,[b] deg	Output angle,[d] deg
1	3.8	-5.6
2	0	2.9
3	6.4	-5.6
4	-7.0	-1.4
5	4.8	-4.6
6	-2.7	4.9
7	7.2	-3.1
8	4.4	-1.5
9	-4.0	1.7
10	.5	.4
11	2.3	-1.3
12	10.7	-6.7
13	-.1	1.8
14	-6.1	4.5
15	3.0	3.0
16	4.4	-.9
17	.2	3.3
18	3.7	.7
19	-1.4	1.7
20	.6	2.6
21	-4.0	2.0
22	-3.6	.8
23	.3	2.5
24	-2.8	2.2
25	3.8	4.1
26	-1.3	2.1
27	-.4	2.8
28	-2.8	1.5
29	-2.8	.7
30	-2.1	1.6
31	-1.8	1.7
32	-1.9	1.4

[a]In order of increasing kinetic energy.
[b]For centroid of charge; average radius, $\overline{r}$, 0.082 cm.
[c]For centroid of charge; average radius, $\overline{r}$, 0.16 cm.
[d]For centroid of charge; average radius, $\overline{r}$, 0.25 cm.

TABLE II. - ANALYTICAL PERFORMANCE OF VARIAN TWT WITH FIRST DESIGN, 2.4-CENTIMETER-DIAMETER, FOUR-STAGE DEPRESSED COLLECTOR WITH TWT OPERATING AT SATURATION AND DESIGN CASE REFOCUSING

[Computed trajectories shown in fig. 6. Voltages, currents, and powers in percent of V_0, I_0, and V_0I_0, respectively.]

(a) MDC performance

Collecting element	Voltage with respect to ground	Analytical		
		Current	Recovered power	Kinetic power dissipated
TWT body (interception)	0	0	0	0
TWT body (backstreaming)	0	0	0	0
Electrode:				
0 (backstreaming)	0	0	0	0
1	31	32.5	10.1	5.7
2	47	36.7	17.1	8.6
3	85	23.2	19.8	2.1
4	100	7.5	7.5	1.9
Collector efficiency, percent			74.8	

(b) Final power distribution

	Analytical
Total rf power conversion (includes circuit and sever losses)	27.3
Beam interception losses	0
Backstreaming to TWT body	0
MDC dissipation (includes backstreaming to electrode 0)	18.4
Recovered power	54.5

TABLE III. - ANALYTICAL AND EXPERIMENTAL PERFORMANCES OF VARIAN TWT WITH FIRST DESIGN, 2.4-CENTIMETER-DIAMETER, FOUR-STAGE DEPRESSED COLLECTOR WITH TWT OPERATING AT SATURATION AND ACTUAL REFOCUSING

[Computed trajectories shown in fig. 7. Voltages, currents, and powers in percent of V_0, I_0, and V_0I_0, respectively.]

(a) MDC performance

Collecting element	Voltage with respect to ground	Analytical			Experimental		
		Current	Recovered power	Kinetic power dissipated	Current	Recovered power	Kinetic power dissipated
TWT body (interception)	0	0	0	0	5.9	0	[a]4.4
TWT body (backstreaming)	0	9.4	0	3.8	5.1	0	(b)
Electrode:							
0 (backstreaming)	0	3.1	0	1.7	2.8	0	1.8
1	39	36.9	14.3	7.1	34.5	13.3	5.2
2	53	20.6	10.8	4.2	20.0	10.5	3.5
3	81	24.4	19.9	3.6	30.7	25.0	5.6
4	100	5.6	5.6	1.6	1.2	1.2	1.4
Collector efficiency, percent		69.6			69.9		

(b) Final power distribution

	Analytical	Experimental
Total rf power conversion (includes circuit and sever losses)	27.3	[a]23.9
Beam interception losses	0	[a]4.4
Backstreaming to TWT body	3.8	(b)
MDC dissipation (includes backstreaming to electrode 0)	22.1	17.6
Recovered power	50.6	50.1

[a]Using $V_0I_B(1 - \eta_e)$ for the average power of the intercepted electrons.
[b]Not measured.

TABLE IV. - ANALYTICAL AND EXPERIMENTAL PERFORMANCES OF VARIAN TWT WITH SECOND DESIGN, 2.4-CENTIMETER-DIAMETER, FOUR-STAGE DEPRESSED COLLECTOR AND TWT OPERATING AT SATURATION

[Computed trajectories shown in fig. 8. Voltages, currents, and powers in percent of V_0, I_0, and V_0I_0, respectively.]

(a) MDC performance

Collecting element	Voltage with respect to ground	Analytical			Experimental		
		Current	Recovered power	Kinetic power dissipated	Current	Recovered power	Kinetic power dissipated
TWT body (interception)	0	0	0	0	5.9	0	[a]4.5
TWT body (backstreaming)	0	6.9	0	2.8	5.2	0	(b)
Electrode:							
0 (backstreaming)	0	0	0	0	1.7	0	1.4
1	39	38.1	14.8	5.7	34.0	13.2	4.9
2	53	26.5	13.8	5.5	20.7	10.9	4.0
3	81	23.1	18.8	3.5	31.1	25.3	5.3
4	100	5.6	5.6	1.5	1.1	1.1	1.1
Collector efficiency, percent		73.5			71.3		

(b) Final power distribution

	Analytical	Experimental
Total rf power conversion (includes circuit and sever losses)	27.3	[a]24.3
Beam interception losses	0	[a]4.5
Backstreaming to TWT body	2.8	(b)
MDC dissipation (includes backstreaming to electrode 0)	19.1	16.6
Recovered power	53.0	50.4

[a]Using $V_0I_B(1 - \eta_e)$ for the average power of the intercepted electrons.
[b]Not measured.

TABLE V. - ANALYTICAL AND EXPERIMENTAL PERFORMANCES OF VARIAN TWT WITH THIRD DESIGN, 2.4-CENTIMETER-DIAMETER, FOUR-STAGE DEPRESSED COLLECTOR AND TWT OPERATING AT SATURATION

[Computed trajectories shown in fig. 9. Voltages, currents, and powers in percent of V_0, I_0, and V_0I_0, respectively.]

(a) MDC performance

Collecting element	Voltage with respect to ground	Analytical			Experimental		
		Current	Recovered power	Kinetic power dissipated	Current	Recovered power	Kinetic power dissipated
TWT body (interception)	0	0	0	0	5.9	0	[a]4.5
TWT body (backstreaming)	0	3.1	0	1.4	3.5	0	(b)
Electrode:							
1	39	44.4	17.2	5.8	39.8	15.4	5.1
2	53	28.1	14.8	6.8	25.3	13.3	4.9
3	81	20.6	16.8	4.2	25.2	20.5	5.4
4	100	3.7	3.7	1.1	0.4	0.4	3.5
Collector efficiency, percent		73.0			70.2		

(b) Final power distribution

	Analytical	Experimental
Total rf power conversion (includes circuit and sever losses)	27.3	[a]24.4
Beam interception losses	0	[a]4.5
Backstreaming to TWT body	1.4	(b)
MDC dissipation	19.4	18.9
Recovered power	52.5	49.6

[a]Using $V_0I_B(1 - \eta_e)$ for the average power of the intercepted electrons.
[b]Not measured.

TABLE VI. - ANALYTICAL AND EXPERIMENTAL PERFORMANCES OF VARIAN TWT WITH FOURTH DESIGN, 2.4-CENTIMETER-DIAMETER, FOUR-STAGE DEPRESSED COLLECTOR AND TWT OPERATING AT SATURATION

[Computed trajectories shown in fig. 10. Voltages, currents, and powers in percent of V_0, I_0, and V_0I_0, respectively.]

(a) MDC performance

Collecting element	Voltage with respect to ground	Analytical			Experimental		
		Current	Recovered power	Kinetic power dissipated	Current	Recovered power	Kinetic power dissipated
TWT body (interception)	0	0	0	0	5.9	0	[a]4.4
TWT body (backstreaming)	0	3.1	0	1.4	5.5	0	(b)
Electrode:							
1	39	34.4	13.1	4.3	32.2	12.5	4.3
2	53	33.7	17.7	6.6	21.8	11.5	3.4
3	81	21.3	17.3	2.5	33.4	27.2	5.5
4	100	7.5	7.5	2.0	1.3	1.3	2.1
Collector efficiency, percent		76.8			74.3		

(b) Final power distribution

	Analytical	Experimental
Total rf power conversion (includes circuit and sever losses)	27.3	[a]24.4
Beam interception losses	0	[a]4.4
Backstreaming to TWT body	1.4	(b)
MDC dissipation	16.9	15.3
Recovered power	55.9	52.5

[a]Using $V_0I_B(1 - \eta_e)$ for the average power of the intercepted electrons.
[b]Not measured.

TABLE VII. - ANALYTICAL AND EXPERIMENTAL PERFORMANCES OF VARIAN TWT WITH FIFTH DESIGN, 2.4-CENTIMETER-DIAMETER, FOUR-STAGE DEPRESSED COLLECTOR AND TWT OPERATING AT SATURATION

[Computed trajectories shown in fig. 11. Voltages, currents, and powers in percent of V_0, I_0, and V_0I_0, respectively.]

(a) MDC performance

Collecting element	Voltage with respect to ground	Analytical			Experimental		
		Current	Recovered power	Kinetic power dissipated	Current	Recovered power	Kinetic power dissipated
TWT body (interception)	0	0	0	0	5.9	0	[a]4.4
TWT body (backstreaming)	0	3.1	0	1.4	5.0	0	(b)
Electrode:							
1	39	33.1	12.8	4.1	28.2	10.9	1.8
2	53	32.5	17.1	5.4	26.2	13.8	5.8
3	81	23.7	19.3	3.0	33.8	27.5	3.6
4	100	7.5	7.5	2.0	.9	.9	3.7
Collector efficiency, percent		78.0			75.3		

(b) Final power distribution

	Analytical	Experimental
Total rf power conversion (includes circuit and sever losses)	27.3	[a]24.5
Beam interception losses	0	[a]4.4
Backstreaming to TWT body	1.4	(b)
MDC dissipation	16.0	14.8
Recovered power	56.8	53.1

[a]Using $V_0I_B(1 - \eta_e)$ for the average power of the intercepted electrons.
[b]Not measured.

TABLE VIII. - ANALYTICAL AND EXPERIMENTAL PERFORMANCES OF VARIAN TWT WITH SIXTH DESIGN, 2.4-CENTIMETER-DIAMETER, FIVE-STAGE DEPRESSED COLLECTOR AND TWT OPERATING AT SATURATION

[Computed trajectories shown in fig. 12. Voltages, currents, and powers in percent of V_0, I_0, and V_0I_0, respectively.]

(a) MDC performance

Collecting element	Voltage with respect to ground	Analytical			Experimental		
		Current	Recovered power	Kinetic power dissipated	Current	Recovered power	Kinetic power dissipated
TWT body (interception)	0	0	0	0	5.9	0	[a]4.4
TWT body (backstreaming)	0	3.1	0	1.4	4.2	0	(b)
Electrode:							
1	40	31.2	12.4	3.3	26.2	10.2	3.8
2	48	23.1	11.2	3.3	22.5	10.9	3.3
3	70	11.3	7.9	1.5	7.0	4.9	1.2
4	82	23.7	19.4	2.9	33.7	27.6	4.6
5	100	7.5	7.5	2.0	.5	.5	2.2
Collector efficiency, percent		80.1			76.1		

(b) Final power distribution

	Analytical	Experimental
Total rf power conversion (includes circuit and sever losses)	27.3	[a]24.1
Beam interception losses	0	[a]4.4
Backstreaming to TWT body	1.4	(b)
MDC dissipation	14.5	15.2
Recovered power	58.4	54.1

[a]Using $V_0I_B(1 - \eta_e)$ for the average power of the intercepted electrons.
[b]Not measured.

TABLE IX. - ANALYTICAL AND EXPERIMENTAL PERFORMANCES OF VARIAN TWT WITH SIXTH DESIGN, 2.4-CENTIMETER-DIAMETER, FOUR-STAGE DEPRESSED COLLECTOR AND TWT OPERATING AT SATURATION

[Computed trajectories shown in fig. 13. Voltages, currents, and powers in percent of V_0, I_0, and V_0I_0, respectively.]

(a) MDC performance

Collecting element	Voltage with respect to ground	Analytical			Experimental		
		Current	Recovered power	Kinetic power dissipated	Current	Recovered power	Kinetic power dissipated
TWT body (interception)	0	0	0	0	5.9	0	[a]4.4
TWT body (backstreaming)	0	3.1	0	1.4	5.3	0	(b)
Electrode:							
1	40	31.3	12.6	3.4	24.0	9.6	3.5
2	52	34.4	18.0	5.6	29.6	15.5	4.8
3	81	25.6	21.0	3.7	34.8	28.5	5.4
4	100	5.6	5.6	1.6	.4	.4	2.0
Collector efficiency, percent		78.4			76.1		

(b) Final power distribution

	Analytical	Experimental
Total rf power conversion (includes circuit and sever losses)	27.3	[a]24.1
Beam interception losses	0	[a]4.4
Backstreaming to TWT body	1.4	(b)
MDC dissipation	15.8	15.8
Recovered power	57.2	54.0

[a]Using $V_0I_B(1 - \eta_e)$ for the average power of the intercepted electrons.
[b]Not measured.

TABLE X. - SUMMARY OF ANALYTICAL AND EXPERIMENTAL PERFORMANCES OF VARIAN TWT WITH 2.4-CENTIMETER-DIAMETER, FOUR-STAGE DEPRESSED COLLECTOR AND TWT OPERATING AT SATURATION

MDC design	Analytical MDC efficiency at 4.0 GHz, percent	Experimental MDC efficiency[a] at 4.0 GHz, percent	Experimentally optimized[b] MDC efficiency, percent
1	69.6	69.9	71.6
2	73.5	71.3	73.4
3	73.0	70.2	74.2
4	76.8	74.3	76.3
5	78.0	75.3	77.4
6, (5 stage)	80.1	76.1	79.0
6, (4 stage)[c]	78.4	76.1	78.0

[a]An identical refocusing system and MDC operating conditions to the analytical case.

[b]Experimentally optimized at the operating frequency for maximum η_e (4.75 GHz) by varying the refocusing system profile, collector voltages, and MDC spike length (changes external to the vacuum envelope of the TWT).

[c]Two intermediate electrodes electrically connected and operated as one.

1. Report No. NASA TP-2162	2. Government Accession No.	3. Recipient's Catalog No
4. Title and Subtitle EXPERIMENTAL VERIFICATION OF THE MULTISTAGE DEPRESSED COLLECTOR DESIGN PROCEDURE FOR A HIGH-PERVEANCE, HELIX-TYPE, TRAVELING-WAVE TUBE		5. Report Date May 1983 6. Performing Organization Code 506-61-42
7. Author(s) James A. Dayton, Jr., Henry G. Kosmahl, and Peter Ramins		8. Performing Organization Report No E-1362 10. Work Unit No.
9. Performing Organization Name and Address National Aeronautics and Space Administration Lewis Research Center Cleveland, Ohio 44135		11. Contract or Grant No.
12. Sponsoring Agency Name and Address National Aeronautics and Space Administration Washington, D.C. 20546		13. Type of Report and Period Covered Technical Paper 14. Sponsoring Agency Code

15. Supplementary Notes

16 Abstract

The validity of a computational procedure for the design of multistage depressed collectors (MDC's) is demonstrated for a traveling wave tube (TWT) with a perveance of 1.23×10^{-6}. The MDC is used with spent-beam refocusing to improve substantially the efficiency of the TWT. Previous reports on this subject have verified the MDC design procedure for TWT's with lower perveance under a variety of operating conditions. The design procedure is based on two computer programs that create a mathematical model of the electric and magnetic fields of the TWT-refocuser-MDC system and its electron beam. The two principal outputs of the analysis are a description of the rf performance of the TWT and the trajectories of representative groups of charges from the input of the TWT to their points of interception on the MDC electrodes. The trajectories provide the information from which the collector efficiency can be calculated. The analytical predictions were compared in considerable detail with measured results. Very good agreement was obtained between the analytical and experimental values of collector efficiency. Several design iterations are described. The highest experimentally optimized MDC efficiencies achieved were 79 percent for a five-stage collector and 78 percent for a four-stage collector. The collecting surfaces of the MDC were contained within a cylindrical volume approximately 2.4 cm in diameter and 3.0 cm long.

17. Key Words (Suggested by Author(s))
Microwave tubes
Multistage depressed collectors
Computer-aided design

18. Distribution Statement
Unclassified - unlimited
STAR Category 33

19. Security Classif. (of this report)	20. Security Classif. (of this page)	21. No. of Pages	22. Price*
Unclassified	Unclassified	23	A01

* For sale by the National Technical Information Service, Springfield Virginia 22161

NASA-Langley, 1983